Supporting Information for:

Direct Observation of Oligomerization by Single Molecule Fluorescence Reveals a Multistep Aggregation Mechanism for the Yeast Prion Protein Ure2

Jie Yang[a,e,‡], Alexander J. Dear[b,‡], Thomas C.T. Michaels[b,d], Christopher M. Dobson[b], Tuomas P.J. Knowles[b,c,*], Si Wu[a,e,*] & Sarah Perrett[a,e,*]

[a]National Laboratory of Biomacromolecules, CAS Center for Excellence in Biomacromolecules, Institute of Biophysics, Chinese Academy of Sciences, 15 Datun Road, Chaoyang District, Beijing 100101, China.

[b]Centre for Misfolding Diseases, Department of Chemistry, University of Cambridge, Lensfield Road, Cambridge CB2 1EW, United Kingdom.

[c]Cavendish Laboratory, J J Thomson Avenue, Cambridge CB3 1HE, United Kingdom.

[d]Paulson School of Engineering and Applied Sciences, Harvard University, Cambridge, MA, United States.

[e]University of the Chinese Academy of Sciences, 19A Yuquan Road, Shijingshan District, Beijing 100049, China.

[‡]These authors contributed equally to this work.

*To whom correspondence may be addressed. E-mail: sarah.perrett@cantab.net; wusi@moon.ibp.ac.cn; tpjk2@cam.ac.uk

Supporting information includes:

Additional Methods
Figures S1-S8
Tables (Table S1-S5)

Table of contents

Additional Methods

Fluorescence labeling of Ure2

The single-point cysteine variants V9C, S53C and S68C of Ure2 were labeled with maleimide functionalized Alexa Fluor 488 (AF488), Alexa Fluor 555 (AF555) or Alexa Fluor 647 (AF647) dye (Invitrogen) via the cysteine thiol group according to the requirements of the experiment. The reaction was carried out by incubating protein with a 2-fold molar excess of dye at 25°C for 30 min. Labeled protein was then purified using a P10 desalting column (GE Healthcare) to remove the excess free dye. The dye-to-protein labeling ratio was determined by its absorbance spectrum according to the product instructions and calculated to be 85-95%. Labeled protein was flash-frozen and stored in aliquots at −80°C. Each aliquot was thawed and centrifuged at 18000 *g* to remove any small aggregates immediately before use.

Comparison of fibril formation kinetics of labeled and unlabeled full-length Ure2

A 150 μL sample of 15 μM WT or mutant Ure2 protein supplemented with 10 μM ThT was incubated in a 96-well plate (COSTAR). The ThT fluorescence was monitored using a 96-well SpectraMax M3multimode plate reader (Molecular Devices) under its default shaking mode at 30°C with excitation at 450 nm and emission at 485 nm (Figure S1A). When comparing the fluorescence labeled and unlabeled Ure2, ThT could not be used and the kinetics of fibril formation was measured by turbidity at 400 nm on the plate reader (Figure S1B), under the same conditions as for Figure S1A.

Transmission electron microscopy (TEM)

After the aggregation reaction reached a plateau, 5 μl of each fibril sample was loaded onto carbon-coated copper grids for 1 min and stained with 1% uranyl acetate. A Phillips Tecnai 20 electron microscope at 120 kV was used to observe the morphology of the fibrils formed by WT Ure2 and its variants (Figure S1C).

Intra-dimer FRET measurement of Ure2

Ure2-V9C or Ure2-E268C (which was produced in the same way as the other variants) was labeled with an equimolar mixture of maleimide functionalized Cy3 and Cy5 (GE Healthcare) using the same method as described above. The labeling ratio was determined by its absorbance spectrum according to the product instructions and calculated to be above 90%. The Cy3/Cy5 double labeled Ure2 was mixed with unlabeled Ure2 at a ratio of 1:20 to give a final concentration of 15 μM and incubated to form fibrils in an Eppendorf tube at 30ºC. The FRET spectra of native and fibrillar Ure2 as well as the sonicated fibril seeds were measured on a Shimadzu RF-5301PC fluorimeter before and after the aggregation reaction with excitation at 532 nm and emission ranging from 540 nm to 800 nm.

The labeling sites V9C and E268C are located in the N-terminal and C-terminal domain of Ure2 respectively. The FRET efficiency between the two V9C sites of the native Ure2 dimer was low, while it increased to a high level after conversion to fibrils, consistent with the previous conclusion that the disordered N-terminal of Ure2 reorganizes into compact amyloid structure (Figure S2A). The FRET efficiency between the two E268C sites in the Ure2 dimer remained nearly unchanged after its conversion into amyloid fibrils, indicating that the Ure2 dimer does not dissociate when forming fibrils (Figure S2B). The inter-dimer FRET signal did not decrease for either mutant, as would be expected if dissociation of the dimer occurred during fibril formation, due to exchange

with the 95% excess of unlabeled protein in the mixture. As a control, the FRET spectrum of 7 M GdmCl denatured Ure2 was also measured, representing the case in the absence of FRET. The denatured sample showed extremely low intensity of Cy5 which was mainly caused by direct excitation.

Confocal single-molecule FRET (smFRET) measurement of Ure2 oligomer formation

An equimolecular concentration (15 μM) of AF647-labeled Ure2 was mixed with either AF488-labeled Ure2 or AF555-labeled Ure2 as indicated, and incubated in the dark. In order to have sufficient time to obtain accurate smFRET statistics, we used mild fibril-inducing conditions by incubating the sample tubes in an Innova 4230 incubator (New Brunswick) at 18°C with an agitation rate of 150 rpm to allow one hour intervals to collect single molecule data between each sampling. The same conditions were used to acquire the data shown in Figures 1, 2, 3 and 5. In this setup, the volume of the aggregation reaction system is large enough to allow sampling along the whole reaction time course. During the fibril formation process, a 4 μL aliquot was taken from the sample tube at each time point and diluted 2.5×10^5-fold immediately for smFRET data collection at room temperature. Glass coverslips (Fisher) were pre-cleaned with piranha solution (sulfuric acid: hydrogen peroxide = 3:1) for 30 min at 95°C and washed with distilled water. A silicon gasket (Grace Bio-labs) was pressed and sealed onto the coverslip to limit the sample volume to 300 μL in each measurement. The coverslip surface was coated with 5 μM unlabeled Ure2 protein for 20 min and then removed to prevent adsorption of the sample protein onto the coverslip. In seeding experiments, 1% unlabeled mature fibrils was added to an equimolar mixture of AF555 and AF647 labeled 15 μM Ure2 at the beginning of the fibril formation, and the subsequent manipulations and detection were the same as that of unseeded experiments. As a control, 1% AF555/AF647 labeled mature fibrils was added to the 15 μM unlabeled soluble Ure2 sample to exclude the possibility that the observed oligomers had dissociated from fibrils. In order to compare with the smFRET data, the ensemble amyloid formation of Ure2 was also carried out in a tube under the same incubation conditions as used in the smFRET experiments (Figures 1, 2 and 5); 600 μL of 10 μM ThT was added to the aliquot sample taken from the tube and measured on a HitachiFL-4500 fluorimeter as described previously[1]. In seeded experiments, 1% mature fibrils was added as fibril seed to the 15 μM unlabeled soluble Ure2 sample at the beginning of fibril formation.

SmFRET experiments were carried out using a home-built confocal microscope similar to that described previously[2]. An inverted fluorescence microscope (Ti-E, Nikon) was equipped with a 100× objective (N.A. = 1.4, Nikon). The beam of a 488 nm laser (Coherent) or 532 nm laser (Pavilion) was directed to the back port of the microscope to excite the AF488/AF647 or AF555/AF647 pairs with a laser power of 50 μW or 37.5 μW, respectively. The fluorescence emission was collected via the same objective, filtered with a 50 μm pinhole and split into donor and acceptor channels with ZT640RDC (for AF488/AF647 pair) or T660LPXR (for AF555/AF647 pair) dichroic mirrors (Chroma) before being focused on to two avalanche photodiode detectors (SPCM-AQRH-14, Excelitas) with appropriate fluorescence filters (Chroma, ET525/50 for AF488, ET595/50 for AF555 and ET690/50 for AF647). The fluorescence of labeled sample that freely diffused across the focal volume was simultaneously collected using two avalanche photodiode detectors and recorded using a two-channel photon counting card (PMS-400A, Becker & Hickl) with 1 ms bin time.

The confocal single molecule FRET data was processed using MATLAB (Math Works) and Origin 8.0, and analyzed as described previously with modifications[3,4]. D=5 for the donor channel and A=10 for the acceptor channel was set as the threshold for single molecule bursts to select the oligomer events in AF488/AF647 labeled

smFRET experiments, and D=10 and A=20 was used as the threshold in AF555/AF647 labeled smFRET experiments because of the high signal intensity under this setup. For the case that oligomer burst spanning times were between 2 to 5 bins, only the brightest burst among them was counted and used to calculate both the FRET efficiency and apparent oligomer size. The oligomer bursts spanning more than 5 bins were considered to be insoluble fibrillar species or impurities and were excluded from the analysis. The sample labeled with the AF555 and AF647 pair was used to observe the time-dependent change of oligomer concentration (Figures 1C, 2 and 5). Due to the significant "zero peak" in the AF555/AF647 smFRET experiment, only the bursts with FRET efficiency larger than 0.2 were counted as oligomer events to exclude crosstalk from the tail of the "zero peak". In order to calculate the oligomer concentration for each time point, the 15 μM AF555-labeled soluble Ure2 was diluted 2.5×10^5-fold, and the total burst number within the 1 h detection time in the donor channel was measured and used as a concentration standard. The number of the selected oligomer events was divided by the total number of donor bursts of the AF555-labeled soluble Ure2 to obtain the amount of oligomer as a proportion of the total protein concentration, which was then converted to oligomer concentration using 15 μM AF555-labeled Ure2 as a concentration standard. At least three independent experiments were performed to obtain accurate averaged results.

Since the oligomer events are rare in the solution, the unwanted "zero peak" caused by donor-only free Ure2 species is extremely high, the tail of which could interfere with the real FRET events. Therefore when counting the oligomer number by smFRET using AF555/AF647 labeling, a higher threshold in the acceptor channel than in the donor channel (D=10 and A=20) was used in order to lower the crosstalk between the "zero peak" and real FRET signal from oligomers. We also tried equal threshold in both channels (D=A=10) to select oligomers and did an equivalent kinetic analysis of combined smFRET and ThT data. In this case, the extra oligomer number counts come mostly from the contribution of the tail of the zero peak, especially at the early stages of the aggregation reaction when free Ure2 is at a high concentration. However, the fitting results show no great difference, with the values for k_d, k_c, k_+, and k_{oligo} and k_- within a factor of two of those obtained from the D=10 and A=20 threshold data (Table S1). Therefore, the selection of the threshold does not affect the accuracy of the kinetic analysis or influence the conclusions.

The above smFRET experiments (Figures 1, 2 and 5) were performed using the AF555/AF647 dye pair, as the residual free dye that cannot be removed completely during protein/free dye separation generates a lower background for AF555 than for AF488, producing high quality data suitable for quantitative global kinetic analysis (see below). However, the AF488/AF647 dye pair is more sensitive to conformational changes within the protein aggregates in this system, and allowed detection of distinct oligomer populations by measuring the FRET efficiency distribution within oligomers (Figure 3). The FRET efficiency for each selected oligomer was calculated using the equation below:

$$E_{\mathrm{FRET}} = \frac{I_{\mathrm{A}}}{\gamma I_{\mathrm{D}} + I_{\mathrm{A}}} \qquad \text{(S1)}$$

where I_{A} and I_{D} are the fluorescence intensity of acceptor and donor respectively, and γ corresponds to the correction factor that accounts for the different quantum yields and detection efficiencies of AF488 and AF647, which was measured to be 0.82 using single labeled protein under our 488/647 detection setup[5]. The statistical FRET distribution histograms of selected oligomer events were generated at each incubation time point and globally fitted to either single or double Gaussian functions to obtain the center value of the peaks (Figure 3A and B).

Total internal reflection fluorescence (TIRF) smFRET measurement of Ure2 fibril dissociation

Labeled fibrils were prepared by incubating an equimolar mixture of AF488-labeled Ure2 and AF647-labeled Ure2 under the same conditions used in the aggregation experiments. The final fibrils were centrifuged and washed three times with 50 mM Tris-HCl (pH 8.4) buffer containing 200 mM NaCl. The pellet was then gently resuspended in 300 μL buffer and sonicated (Sonics and Materials VCX750) for a total time of 30 s (5 s bursts) at 30 percent power. A 4 μL sample was taken from the sonicated fibrils, diluted to a concentration suitable for single molecule detection and loaded onto the microscope coverslip. The protein aggregates were then absorbed to coverslips and observed by TIRF microscopy. In order to diminish the photobleaching and blinking of the fluorophore, an enzymatic deoxygenation system containing 0.8% glucose, 100 μg/mL glucose oxidase, 20 μg/mL catalase, and 1.5 mM Trolox (Sigma) was added in the final imaging solution as described previously[6].

The objective-based smFRET TIRF instrument was built on a Nikon Ti-E inverted microscope equipped with a 100× TIRF objective (Apo TIRF, N.A. = 1.49, Nikon). A 0.3 mW 488 nm laser (Coherent) was used to illuminate a region of 70 μm diameter and excite the labeled protein on the surface of coverslips. The fluorescence emission was separated by DualView optics (Photometrics) to donor and acceptor channels using a FF01-535/50 band pass filter (Semrock) and an ET655LP long pass filter (Chroma) respectively, and then imaged on an EMCCD (Evolve 512, Photometrics); 300 frames of 100 ms integration time were acquired for each region and more than 70 regions were observed for each sample. Data analysis of smFRET TIRF images was performed with the assistance of the open source iSMS software written in MATLAB[7] to generate the FRET efficiency distribution histogram (Figure 4). The FRET efficiency of each frame was calculated according to Eq. S1 with the γ factor measured to be 0.82 according to the established method[6] under the current TIRF setup.

Detailed description of the kinetic model

The experimentally-measurable quantities that we seek to model are the total oligomer concentration $O(t)$, and the concentration of dimers that have been incorporated into fibrils, called the fibril "mass concentration" $M(t)$. We have established the main reaction processes acting on these quantities in the main text: oligomer formation from dimers; oligomer dissociation back to dimers; oligomer conversion into fibrillar aggregates; elongation of fibrillar aggregates through dimer addition; and fragmentation of fibrils into smaller fibrils. We model the total oligomer concentration despite the existence of two oligomer sub-populations because, as explained in the Methods section of the main text, our data on sub-populations of oligomers is of insufficient completeness and accuracy for kinetic modelling. Our model is thus partially coarse-grained. This modelling approach is rigorously justified in the SI section "Interpreting the kinetic model", in which we also demonstrate that the effects of the coarse-graining are largely limited to the "conversion" step, which contains information on the interconversion of distinct oligomer species as well as their ultimate conversion to growing fibrils. This is analogous to the coarse-grained "primary nucleation" step in traditional bulk models of fibrillar growth that actually contains information on all of the oligomeric reactions that lead to new fibril formation.

We note for full rigor here that we have ignored depolymerization, as at equilibrium the dimer concentration is very low (less than 2% as calculated from the single molecule burst density of donor-labeled Ure2 after the aggregation reaction reached plateau) and thus this process does not significantly affect the kinetics. We have also ignored fibril annealing, as it has a negligible effect on the time profile of the measured quantities $M(t)$ and $O(t)$. Furthermore, we may ignore the changes in dimer concentration caused directly by the oligomer formation and depletion processes, as these are insignificant relative to the changes due to fibril elongation, due to the low

incidence of oligomers relative to native Ure2 dimers. According to the law of mass action, the rate of a reaction is proportional to the product of the concentrations of the species involved. Neglecting certain other small terms[8], we can therefore write the rate equations for our aggregating system, outlined in the main text (Eq. 1-4):

$$\frac{dO}{dt} = k_{\mathrm{oligo}} m(t)^2 - k_{\mathrm{c}} O(t) - k_{\mathrm{d}} O(t) \qquad (1)$$

$$\frac{dP}{dt} = k_{\mathrm{c}} O(t) + k_{-} M(t) \qquad (2)$$

$$\frac{dM}{dt} = 2k_{+} m(t) P(t) \qquad (3)$$

$$\frac{dm}{dt} = -2k_{+} m(t) P(t) \qquad (4)$$

In order to describe the kinetics of $M(t)$ and $O(t)$ with a closed set of rate equations, it was necessary to also include an explicit rate equation for the fibril concentration $P(t)$, and for the dimer concentration $m(t)$. This is because oligomer formation from dimers depends in general on dimer concentration, and fibril elongation by dimer addition will depend explicitly on fibril concentration and dimer concentration.

Each process of importance is now represented by a rate term in the above closed set of rate equations: fibril elongation by $2k_{+}m(t)P(t)$; fibril fragmentation (proportional to the total concentration of potential break sites, and therefore to the fibril mass concentration) by $k_{-}M(t)$; oligomer dissociation by $k_{\mathrm{d}}O(t)$; oligomer conversion by $k_{\mathrm{c}}O(t)$; and oligomer formation by $k_{\mathrm{oligo}}m(t)^2$.

Choosing reaction orders

We do not know the reaction orders of the oligomer formation and conversion processes with respect to dimer concentration for certain *a priori*. We can see from the shape of the oligomer concentration curves that the reaction order of oligomer formation, n_{o}, with respect to dimers must be at least 1, and unlikely to exceed 5; however, since our dataset involves only one initial dimer concentration, we cannot more accurately determine it from fitting. Including the reaction order as a free parameter in the model would therefore be overfitting, and we must choose a value before proceeding with the data fitting. We believe 2 is a physically reasonable value given that we expect that all oligomers must either arise from the initial interaction of a pair of dimeric Ure2 molecules (i.e. formation of a "dimer-of-dimers"), or have grown from dimers-of-dimers through dimer addition, so the only reaction that forms new oligomers is the dimer-of-dimer formation reaction. In fact, it is hard to physically justify a reaction order substantially differing from this.

Any error in our choice of reaction order relative to the "true" value is expected to have no qualitative effect on the modelling conclusions, for the same reason as why we were forced to choose an *a priori* value in the first place – for this limited dataset, all physical choices of reaction order will result in similar fit quality and similar parameters. This is provided we realize that with a varying reaction order we must compare values of $k_{\mathrm{oligo}}m(0)^{n_{\mathrm{o}}}$, not k_{oligo}.

By fitting to a single initial dimer concentration it is not possible to determine the reaction order accurately for the oligomer conversion step either. In fact, the conversion reaction order, n_{p}, is even less visible from analysis of datasets with a single initial dimer concentration, since conversion is of principal importance early in the reaction before significant dimer depletion has occurred. We must therefore again choose a reaction order with respect to dimers; we have chosen zero. As before, the value chosen has no effect on the modelling, beyond a

redefinition of the rate constant k_c, provided it is understood that the relevant fitting parameter to compare is really $k_c m(0)^{n_p}$ and not simply k_c.

We verified the insensitivity of the modelling of our available data to these reaction orders by carrying out the fitting procedure with alternative values for the reaction orders, and examining the variability of the fitted rate parameters. For oligomer formation we expect that the only physically reasonable alternatives are between 1 and 2 (as would be seen in the case of saturation effects). We think it is highly unlikely to be greater than 3; therefore, we trialed 1, 2, and 3. The initial slopes of the oligomer concentrations for each Ure2 mutant are very similar, making it extremely unlikely that their formation reaction orders are different; thus, we limit our analysis to considering identical reaction orders for each mutant.

In the case of conversion, we trialed reaction orders of 0, 1 and 3. This time we have no reason to suppose they are the same for each mutant. We find that, to within error, our key fitting results are totally unaffected by changes in conversion reaction order, even when the mutants have different reaction orders (recall that k_- and k_c can only be determined to within an order of magnitude). We further find that changes in the reaction order of oligomer formation have only small quantitative effects on k_{oligo} and k_d for each mutant, but do not affect their ratio to within error, or any of our other key conclusions. We are therefore satisfied that the precise values of these reaction orders are unimportant for our analysis. See Tables S2-S5 for full results of the sensitivity analysis.

Analytical solution for the aggregation kinetics

At early times, the dimer concentration can be considered to be approximately constant at its initial value $m(0)$ and our kinetic rate equations Eq. 1-3 (above and in main text) reduce to a simpler form:

$$\frac{d}{dt}O^{(0)}(t) = \alpha - k_1 O^{(0)}(t) \qquad \text{(S2)}$$

$$\frac{d}{dt}P^{(0)}(t) = k_c O^{(0)}(t) + k_- M^{(0)}(t) \qquad \text{(S3)}$$

$$\frac{d}{dt}M^{(0)}(t) = 2k_+ m(0) P^{(0)}(t) \qquad \text{(S4)}$$

where $k_1 = k_c + k_d$, and $\alpha = k_{oligo} m(0)^2$. These can be solved for unseeded initial conditions to give early-time analytic expressions. We know from experiment that oligomers are present only at low concentration, and therefore that dissociation is relatively fast. This allows us to simplify our early-time analytical expressions to give:

$$O^{(0)}(t) = \frac{\alpha}{k_1}(1 - e^{-k_1 t}) \qquad \text{(S5)}$$

$$P^{(0)}(t) = \frac{\alpha k_c}{2\kappa(k_1 + \kappa)}(e^{\kappa t} - 1) \qquad \text{(S6)}$$

where $k_1 = k_c + k_d$ and $\kappa = \sqrt{2k_+ k_- m(0)}$. Now, using conservation of mass, $M(t) = m(0) - m(t)$, we rewrite our equation for fibril mass concentration as an integral equation for the dimer concentration:

$$m(t) = m(0) \exp\left(-2k_+ \int_0^t P(t')dt'\right) \qquad \text{(S7)}$$

Substituting our early-time expression $P^{(0)}(t)$ into the right-hand side, and again applying conservation of mass, yields a 1st order self-consistent expression for $M(t)$ of remarkable accuracy, in line with Ref. 8 and 9:

$$M^{(1)}(t) = m(0)(1 - \exp(-A(e^{\kappa t} - 1))) \qquad \text{(S8)}$$

with $A = \frac{\alpha k_+ k_c}{\kappa^2 (k_l + \kappa)}$. This expression bears a striking resemblance to the expressions derived in Ref. 10 for the kinetics of fragmenting systems. This is to be expected given that oligomers do not comprise a large proportion of the system mass. Note that the parameters k_+, k_- and k_c cannot therefore be uniquely determined from fitting bulk aggregate mass concentration to this expression.

Interpreting the results of data fitting to the kinetic model

The model in the main text was selected because it is the simplest possible physically reasonable model capable of fitting the available combined smFRET/ThT experimental data with reasonable accuracy. This is in line with the principle of parsimony that underlies the theory of model selection[11]. The success of the fits demonstrates that, at this level of experimental detail, the full range of low- and high-FRET oligomers of all sizes, and the reactions that connect them, can be well-approximated by a single oligomer species undergoing the formation, dissociation and conversion processes currently incorporated in the model. This is inferred, not assumed. The inclusion of any finer detail in a kinetic model would lead to overfitting, degrading the quality of subsequent inferences made on the basis of the model. It would only be reasonable to test such models given a much larger dataset than is currently available.

Nonetheless, it is of interest to investigate how exactly we might interpret our coarse-grained model reaction processes in terms of more fundamental reaction steps expected to be present, and to what extent they might hold up as true constants in a more detailed study. We know from smFRET data (Figure 3) that there are in fact two distinct structures of oligomer, distinguished by their differing FRET efficiencies, and that high-FRET oligomers likely form from low-FRET oligomers and not directly from dimers. Therefore, the total oligomer formation step in the model is likely indeed a fundamental reaction step: that of low-FRET oligomer formation. We also know that at early and intermediate times, low-FRET oligomers dominate the population; thus, even if some high-FRET oligomers were to form directly from dimers, the fitted total oligomer formation rate constant would still be a very good approximation to the low-FRET oligomer formation rate constant.

To investigate what range of sizes oligomers might come in, a size distribution analysis was performed, that indicates that both low-FRET and high-FRET oligomer populations have average apparent sizes that change little during the majority of the time course of the aggregation reaction (Figure S6); implying that the normalized size distribution of each population remains constant. Therefore, the time evolution of the full network of oligomeric species should be faithfully represented by a kinetic model which treats the low-FRET oligomers and the high-FRET oligomers each as a single kinetic species, since the coarse-grained rate constants should remain approximately constant throughout the reaction. The experiments on low/high-FRET oligomers indicate that the majority of oligomer depletion is low-FRET oligomer dissociation; we may therefore identify the total oligomer dissociation rate constant with the low-FRET oligomer dissociation rate constant.

We expect the coarse-grained total oligomer conversion step to contain information both on interconversion of low- and high-FRET oligomers, and the ultimate conversion of high-FRET oligomers to growing fibrils. To

interpret it more quantitatively, we start by explicitly writing down the more detailed kinetic model that we believe governs the system:

$$\frac{dS_1}{dt} = k_{\text{oligo}} m(t)^2 - (k_{\text{c1}} + k_{\text{d1}}) S_1(t) \quad \text{(S9)}$$

$$\frac{dS_2}{dt} = k_{\text{c1}} S_1(t) - (k_{\text{d2}} + k_{\text{c2}}) S_2(t) \; + k_{\text{L}} P(t) \quad \text{(S10)}$$

$$\frac{dP}{dt} = k_{\text{c2}} S_2(t) + k\_ M(t) \quad \text{(S11)}$$

$$\frac{dM}{dt} = 2\, k_{+} m(t) P(t); \quad M(t) + m(t) = m(0) \quad \text{(S12)}$$

where $k_{\text{c1}}S_1(t)$ is the rate of conversion of low-FRET to high-FRET oligomers (whose concentrations are given by $S_1(t)$ and $S_2(t)$ respectively); and $k_{\text{c2}}S_2(t)$ is the rate of conversion of high-FRET oligomers to fibrils; we have shown in the main text that these processes likely occur; and $k_{\text{d1}}S_1(t)$ and $k_{\text{d2}}S_2(t)$ are the rates of dissociation of low- and high-FRET oligomers, respectively. Fibril depolymerization experiments outlined in the main text imply that reverse conversion of high- to low-FRET oligomers is not a major process. The rate "constants" k_{c1} and k_{c2} may have dimer dependence (i.e. $k_{\text{c1}}m(t)^{n_1}$). We show in the main text that the basal oligomer concentrations seen at the end of the aggregation reactions are likely due to disaggregation of high-FRET oligomers from fibrils; we represent this here with $k_{\text{L}}P(t)$.

The concentration of $S_2(t)$ changes very little through most of the reaction compared to the other species featuring in these equations, as well as being much lower than $S_1(t)$; thus, applying the steady state approximation and setting its rate of change to zero is reasonable. This gives us:

$$S_2(t) = \frac{k_{\text{c1}}}{k_{\text{c2}} + k_{\text{d2}}} S_1(t) \; + \; \frac{k_{\text{L}}}{k_{\text{c2}} + k_{\text{d2}}} P(t) \quad \text{(S13)}$$

$$O(t) = S_1(t) + S_2(t) = \frac{k_{\text{c1}} + k_{\text{c2}} + k_{\text{d2}}}{k_{\text{c1}}} S_2(t) \; - \; \frac{k_{\text{L}}}{k_{\text{c1}}} P(t) \quad \text{(S14)}$$

$$\frac{dP}{dt} = \frac{k_{\text{c1}} k_{\text{c2}}}{k_{\text{c1}} + k_{\text{c2}} + k_{\text{d2}}} O(t) + k\_ M(t) \; + \; \frac{k_{\text{L}} k_{\text{c2}}}{k_{\text{c1}} + k_{\text{c2}} + k_{\text{d2}}} P(t) \quad \text{(S15)}$$

If we compare to the coarse-grained equations in the main text, we can identify the coarse-grained "k_{c}" in the steady-state limit to be approximately equal to $\frac{k_{\text{c1}}k_{\text{c2}}}{k_{\text{c1}}+k_{\text{c2}}+k_{\text{d2}}}$. This can be simplified given that $S_2(t) \ll S_1(t)$, and so $k_{\text{c2}} + k_{\text{d2}} \gg k_{\text{c1}}$. In fact, as we know most oligomers do not become fibrils, we likely have $k_{\text{d2}} \gg k_{\text{c2}}$, and so our interpretation of conversion becomes $k_{\text{c}} \simeq k_{\text{c1}}k_{\text{c2}}/k_{\text{d2}}$, i.e. the coarse-grained "conversion" rate constant is proportional to those for both fine-grained conversion steps. We can furthermore identify late-time underestimate of the total oligomer concentration data by the coarse-grained model as being due to the neglected term proportional to $P(t)$, as expected.

These results are essentially unchanged for non-zero conversion reaction orders – the rate constants k_{c1} and

k_{c2} are simply replaced by $k_{c1}m(t)^{n1}$ and $k_{c2}m(t)^{n2}$. Given that conversion is of principal importance early in the reaction before significant dimer depletion has occurred, the reaction orders of conversion would be practically invisible from analysis of datasets involving only a single initial dimer concentration, even if we had separate datasets on low- and high-FRET oligomers of sufficient detail to model.

Bulk concentration-variable kinetic assay and analysis of Ure2 fibril formation

For global kinetic analysis (Figure S4), 150 μL of Ure2 protein solution of different concentrations (2.5 μM – 22.5 μM) supplemented with 5 μM ThT was pipetted into a 96-well clear bottomed plate. The amyloid formation of Ure2 was carried out in a Fluostar Omega plate reader (BMGLabtech) at 30°C with 200 rpm orbital shaking. The ThT fluorescence of each well was read every 15 min with a 450 nm excitation filter and a 485 nm emission filter mounted inside the plate reader. At least three replicates were performed to check the reproducibility and 3-5 repetitions were used for global fitting analysis.

Kinetic analysis was performed with the assistance of an online fitting platform, AmyloFit[12]. In brief, the ThT curves of amyloid formation for Ure2 were normalized, and the time to half-completion ($t_{1/2}$) of each curve was plotted against initial concentration of Ure2 according to the power-law, the slope of which gave the scaling exponent γ. Here, we used the dimer concentration of Ure2 because Ure2 seldom dissociates into monomers either in its native state or during fibril formation, as indicated both by previous studies[13,14] and our intra-dimer FRET experiment (see Figure S2). The slopes of the half-time plots are close to 0.5 (0.64 for WT Ure2, 0.57 for S68C and 0.60 for V9C as shown in Figure S4A), suggesting a fragmentation-dominant mechanism[15]. The concentration-variable ThT curves were therefore fitted globally to a fragmentation-dominant model[10] to obtain the kinetic parameters for fibril formation of WT, Ure2-S68C and V9C, allowing comparison of the differences between them (Figure S4B-D). The normalized ThT data were fitted globally to an analytical solution of the kinetics of breakable filament assembly[10,16]. In this framework, the evolution of the fibril mass concentration is given in terms of the rate constants as a double exponential form as shown:

$$\frac{M(t)}{m_{\mathrm{tot}}} = 1 - \exp\left(-C_{+}e^{\kappa t} + C_{-}e^{-\kappa t} + \frac{\lambda^2}{\kappa^2}\right) \qquad \text{(S16)}$$

where $M(t)$ is the concentrations of protein in fibrillar form at time t, m_{tot} is the total concentration of Ure2 and the constants, C_{+} and C_{-}, are fixed by the initial conditions.

$$C_{\pm} = \pm\frac{\lambda^2}{2\kappa^2} \qquad \text{(S17)}$$

The λ and κ are two combined kinetic parameters related to the primary nucleation rate k_{n}, fibril elongation rate k_{+} and fibril fragmentation rate k_{-}.

$$\lambda = \sqrt{2k_{+}k_{\mathrm{n}}m(0)^{n_{\mathrm{c}}}} \qquad \text{(S18)}$$

$$\kappa = \sqrt{2k_{+}k_{-}m(0)} \qquad \text{(S19)}$$

By globally fitting the normalized ensemble kinetics data, the combined parameters $k_{+}k_{\mathrm{n}}$ and $k_{+}k_{-}$were obtained for each mutant and shown in the figures. k_{n}/k_{-} could be obtained by the ratio of the above two parameters. As the fragmentation rate of the two mutants under the same shaking conditions was the same (see Figure S7 and below), the ratios of the nucleation rates $k_{\mathrm{n}}(S68C)\,/\,k_{\mathrm{n}}(V9C)$ and the elongation rates $k_{+}(S68C)/k_{+}(V9C)$ were calculated and compared. The results show that the elongation rate of Ure2-S68C is 2.3-fold greater than that of V9C, and the amyloid nucleation rate of Ure2-S68C is about 2-fold greater than that for V9C under these experimental conditions.

Dot blot assay

The N-terminal prion domain (PrD) fragment of Ure2 (residues 1-93) was constructed by PCR from the full length Ure2 template using forward primer 5'-CAT GCC ATG GGG GGT TCT CAT C-3' and reverse primer 5'-CC CAA GCT TTA GTC AGA GAA AGC-3'. The PCR product was digested by NcoI and HindIII and ligated into the pET-28a vector. The PrD fragment with His_6-tag was expressed in BL21(DE3) cells. Cells were grown in 2YT medium at 37°C, induced with 1 mM IPTG when the OD_{600} reached 0.6, and allowed to grow for a further 16 h. The PrD protein was purified by nickel-affinity chromatography under denaturing conditions where 7 M GdmCl (Amresco) was added to the same buffer used in the purification of full length Ure2 (50 mM Tris-HCl, 200 mM NaCl, pH 8.4). After purification by Ni affinity column, the eluted protein was concentrated and loaded onto a 24 mL Superdex 200 10/300 GL column (GE Healthcare) for further purification by size exclusion chromatography. Only the monomer peak was collected for further use. Protein purity was checked by SDS-PAGE, and the protein concentration was determined by bicinchoninic acid (BCA) assay kit (Pierce).

The antibody A11 was used to probe relatively disordered oligomeric species, while the antibody OC can recognize β-sheet-containing oligomers and mature fibrils[17]. A11 and OC antibodies show reactivity with oligomers of diverse amyloidogenic proteins including Aβ, α-synuclein, IAPP and the yeast prion Sup35[18,19], suggesting that they recognize certain conformations rather than specific sequences.

The denatured PrD was concentrated using a micro-concentrator tube (Millipore) and diluted 20-fold into 50 mM Tris-HCl (pH 8.4) containing 200 mM NaCl to obtain the final concentration of 30 μM and initiate the fibril formation. A 150 μL sample supplemented with 10 μM ThT was pipetted into the 96-well plate. Fibril formation of the PrD was measured on a Fluostar Omega plate reader (BMGLabtech) at 30°C with 200 rpm orbital shaking. The same batch of PrD protein without adding ThT was also allowed to form fibrils in parallel under the same conditions. The dot blot experiment was performed using a similar procedure to the protocol provided with the antibody. Briefly, during the early stages of the aggregation reaction, 3 μL samples were taken at different time intervals and spotted onto the nitrocellulose membrane. The membrane was blocked by soaking in 5% skimmed milk for 1.5 h and incubated with primary antibody A11 (Abcam, 1:250), OC (Millipore, 1:1000), or anti-Ure2 (1:5000) for 1.5 h at room temperature. The membrane was then washed three times with TBST buffer and incubated with secondary antibody conjugated with HRP. Proteins were visualized using the CLINX ChemiScope 3300 Minichemiluminescence system.

The A11-reactive oligomers appeared during the lag phase and quickly disappeared after the fibril assembly began, while the OC-reactive species gradually increased throughout the measurement (Figure S5). These results show that two types of oligomers exist during Ure2 fibril formation and the concentration of relatively disordered oligomers (A11 reactive) reaches a peak earlier than the β-sheet-rich oligomers (OC reactive), indicating possible conversion from the former to the latter, consistent with our conclusions based on smFRET results.

Size distribution analysis of oligomers

The apparent oligomer size was obtained using the following equation in a similar manner as previously described[3]. For each oligomer burst, the apparent size was calculated by dividing the total intensity of the burst (donor intensity plus acceptor intensity corrected by γ factor) by the average intensity of AF488-labeled native Ure2 in the donor channel, using the equation:

$$\text{Apparent oligomer size} = 4\left(\frac{I_{\mathrm{D}} + I_{\mathrm{A}}/\gamma}{< I_{\mathrm{nativeUre2}} >}\right) \qquad \text{(S20)}$$

The factor of 4 accounts for the fact that only half of the monomers within an oligomer are donor labeled and that the native Ure2 assembles into fibrils as a dimer unit. So the resulting oligomer size is in monomers. The average sizes of low-FRET oligomer (FRET efficiency < 0.5) and high-FRET oligomer (FRET efficiency > 0.5) are calculated respectively and plotted against aggregation time (Figure S6).

Using these intensity-based statistics, a precise oligomer size cannot be obtained due to the different paths taken by the oligomers as they diffuse across the focal volume of the instrument. Moreover, since the fluorescence lifetime measurement of labeled Ure2 indicates a dye-quenching effect within oligomers (see the following section), we could not directly compare the sizes of low-FRET and high-FRET oligomers. However, it still provides an apparent oligomer size which can be used to compare the relative size of oligomers at different time points or for different mutants. The size distribution analysis (Figure S6) indicates that the sizes of low-FRET oligomers and high-FRET oligomers at different time points remain constant throughout the aggregation reaction and there are no obvious differences in the size distribution of the oligomers between the two mutants Ure2-S53C and V9C.

Fluorescence lifetime measurements and analysis

To investigate whether there is a dye-quenching effect within Ure2 oligomers, we performed fluorescence lifetime measurements of AF488 and AF647 by time-correlated single photon counting (TCSPC). Time-resolved fluorescence measurements of AF488 were performed on a HORIBA Scientific DeltaFlex TCSPC system equipped with a DeltaDiode 425 nm pulsed laser as excitation source giving a FWHM around 70 ps. A fluorescence emission filter FF01-535/50 (Semrock) was inserted in front of the detector to collect the signal of AF488. The fluorescence lifetime measurements of AF647 were performed on an FLS920 spectrometer (Edinburgh Instruments) with excitation at 635 nm and emission detection at 670 nm. Photon histograms were recorded until the counts reached 10000 at the maximum. The fluorescence lifetime of AF488 or AF647 of the supernatant and fibrillar species of the aggregation product of an equimolar mixture of AF488 and AF647 labeled Ure2 was measured, after the fibril formation reached a plateau. The fluorescence decay of AF488-labeled native Ure2 or AF647-labeled native Ure2 were also measured as a control in the absence of FRET. The instrument response was measured using scattered light from blank buffer containing no fluorescence labeled sample. The decay traces were fitted to multi-exponential functions using Origin 8 software to obtain the decay time and pre-exponential factors for each component.

The lifetime of AF488 in the supernatant, which contained a low concentration of soluble oligomers and remaining free Ure2, could be fitted to a single-exponential function to obtain a lifetime value of 3.4-3.7 ns. This averaged lifetime is similar to that of AF488-labeled free Ure2 (3.5-3.8 ns). For the resuspended fibrils, the fluorescence lifetime decay curve required fitting to a triple-exponential function giving lifetimes of about 3.3-3.8 ns (8-13%), 1.1-1.4 ns (18-23%) and 0.3-0.4 ns (66-73%). The longest lifetime is similar to that of native Ure2 which should come from the residual native Ure2 or a trace amount of free Ure2 that dissociated from fibrils in the resuspended pellet component, since its amplitude is much lower than the other two components. The lifetime approximate to 1 ns comes from the oligomers that show a FRET effect between the assembled Ure2 within AF488/AF647 oligomers. The shortest 0.3-0.4 ns lifetime of AF488 comes from compact fibrils which indicates dye quenching effects.

The lifetime of the AF647 labeled on Ure2-V9C or S53C is about 1.8-2.1 ns (4.3% and 0.2% for each mutant), which is longer than the measured lifetime of AF647 free dye (1.1 ns), indicating the absence of quenching when attached to the protein. Another much shorter lifetime of about 0.4-0.6 ns (95.7% and 99.8% for each mutant) could be detected in the resuspended fibrils but not in the supernatant, corresponding to the self-quenching effect of the dye. The proportion of the shorter lifetime of AF647 (0.4-0.6 ns, above 90%) is much higher than the proportion of the shortest lifetime of AF488 (0.3-0.4 ns, about 70%). Comparing these two results, the AF647 in the pellet component that has a medium AF488 lifetime (1.1-1.4 ns, about 20%), probably corresponding to high-FRET oligomers, shows a quenching effect. This will cause the size of the high-FRET oligomers to be underestimated, so the apparent size of species with different FRET efficiency could not be directly compared.

Although the fluorescence lifetime results show that partial quenching occurs in fibrils and high-FRET oligomers due to their compact structure, the fluorescence signal is still strong enough to be readily detected in the single molecule experiments. As observed in the smFRET TIRF results, the AF488/AF647 Ure2 fibrils have a strong FRET signal, with an even higher FRET efficiency than the oligomers (Figure 4, high FRET peak with E around 0.8), but these insoluble fibrillar species precipitate out of solution once formed and thus cannot be detected by our confocal smFRET measurements, which only detects species in solution. Further, the concentration of high-FRET oligomers remains almost constant and only accounts for a small proportion of total oligomer (Figure 3). This then explains the lack of rise in FRET signal upon fibril formation in the kinetic experiments (Figures 1, 2, 3 and 5). The observed decrease in the number of Ure2 oligomers is therefore not caused by a quenching effect, but because the oligomers are depleted by other pathways (dissociation back to native dimers or conversion to fibrils).

Analysis of cross-seeded bulk experiments

Bulk cross-seeding experiments (Figure S7) were carried out at 18ºC, in order to investigate whether the difference observed in k_+k_- between the two mutants is due to a difference in k_+. First a batch of S68C seeds were produced and used to seed a solution of native S68C and V9C protein separately, and then the same was done with V9C seeds (Figure S7). The seed concentration was high enough that the initial slope was controlled by elongation. The normalized ThT data were fitted globally to the same model as the unseeded data, but with a non-zero initial fibril concentration, to yield the values of $k_+P(0)$ for each dimer-seed combination, where $P(0)$ is the initial seed fibril concentration. We cannot calculate $P(0)$ exactly, but we can assume its value is the same for reactions using the same seed batch. Therefore the ratios of $k_+P(0)$ for each seed type give us the ratios of the elongation rate constants onto each seed. These ratios were approximately 1.3-1.8:1 for S68C : V9C, added to S68C seeds; and 1:1 for adding to V9C seeds. Had these ratios been the same, this would have provided strong evidence that the elongation rates were seed-independent and that this ratio was therefore also the ratio of self-elongation rates. However, we instead have evidence that elongation is seed-dependent. Furthermore, these results suggest that the elongation rate for S68C is larger than for V9C (note that this is not a conclusive result, as it is technically possible that the rate of addition of V9C dimer onto S68C seed fibril is slower than that of S68C dimer onto V9C seed fibril).

An estimate of the average length of the seed fibrils (100 nm) further allowed us to obtain an order-of-magnitude estimate for $P(0)$, and therefore the absolute elongation rates (approximately $k_+ = 40\ \mu M^{-1}h^{-1}$), and therefore also of the fragmentation and nucleation rates (see main text). Theoretical analysis shows that these

rates are consistent with the formation of extended fibrils.

Fibril length distribution measurement

Measurement of fibril length was based on an imaging method as described previously[20,21]. Fibril formation of 300 μL 15 μM unlabeled Ure2-V9C or Ure2-S68C was performed at 18ºC with an agitation rate of 150 rpm, the same conditions as used in the aggregation reaction monitored by combined ThT assay and smFRET in Figure 5. Once the aggregation reaction reached a plateau, the fibrils were maintained under agitation and 5 μL aliquots of the fibril samples were taken at different plateau time points. The fibrils were imaged using a Tecnai 20 electron microscope at 120 kV following a similar procedure as described above. To avoid fragmentation caused by shear force of the pipette tip, the lower part of the tip was cut before sampling. The TEM images were analyzed using Image J (National Institutes of Health), and the fibril contour length was measured using a segmented line tool. Fibrils extending outside the image board or stacking into clusters were not included. At least 300 fibrils were measured, and two independent sets of measurements were made for each mutant.

Determining fragmentation rates from analysis of fibril length distributions

Fibril length distributions were measured at different time points after completion of the aggregation reaction, as detailed in the above section. From these distributions, the average fibril length was calculated at each time point. Knowing the dimensions of the dimers (a = 1 nm) allows us to convert this to the average number of dimers per fibril, $L(t) = M(final)/P(t)$. Since we know all dimers are converted to fibrils, $M(final) = m_{tot} = 15$ μM, therefore, we can estimate $P(t)$ from the measured average lengths as $P(t) = m_{tot}/L(t)$. Examining the rate equation for $P(t)$ (Eq. (4) in the main text), we find that after aggregation is completed $dP/dt = k_{-}M(final)$. Therefore, the quantity $k_{-}M(final)$ is simply the gradient obtained from fitting $P(t)$ vs t to a straight line. We have carried out this procedure for both variants (see Figure S8A and B), determining that k_{-}, averaged over the two sets of measurements is $k_{-} = (5.1\pm2.3)\times10^{-5}$ h^{-1} for V9C and $k_{-} = (5.4\pm0.5)\times10^{-5}$ h^{-1} for S68C. The difference between these two values is within experimental error, thus justifying our assumption in the main modeling that k_{-} is identical for the two variants.

To further support this conclusion, we have directly analyzed the aggregate length distributions themselves. Analytical solutions to the kinetic equations describing the time evolution of the full length distribution have recently been found (Ref. 21, see Eqs. (12) and (34) therein). These expressions show that, after completion of the aggregation reaction, further time evolution of the distribution is controlled solely by the fragmentation rate. Using the extracted values for the fragmentation rate, we can therefore predict the time course of the full aggregate size distribution using these equations, without introducing additional fitting parameters. The resulting predictions are shown plotted against the data in Figures S8C and S8D, and show overall a good agreement, providing independent validation of the accuracy of the determined fragmentation rate constants.

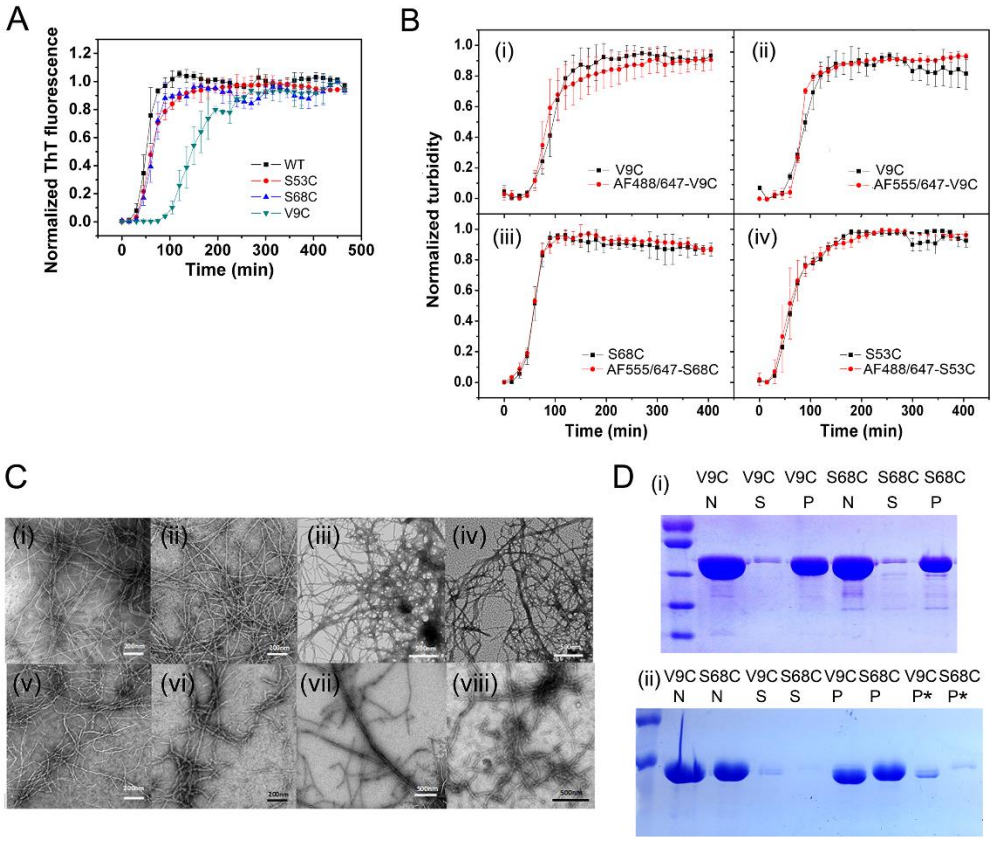

Figure S1. Comparison of fibril formation between Ure2 and its variants. (**A**) Aggregation kinetics of 15 μM WT Ure2 and unlabeled Ure2-V9C, Ure2-S53C and Ure2-S68C measured by ThT fluorescence. The aggregation reactions were carried out in a 96-well SpectraMax M3 multimode plate reader (Molecular Devices) under its default shaking mode at 30°C. The data shown are the average of three replicates, and the error bars represent the standard deviation of the mean. (**B**) Aggregation kinetics of 15 μM (i) unlabeled Ure2-V9C and AF488/AF647 labeled Ure2-V9C, (ii) unlabeled Ure2-V9C and AF555/AF647 labeled Ure2-V9C, (iii) unlabeled Ure2-S68C and AF488/AF647 labeled Ure2-S68C, (iv) unlabeled Ure2-S53C and AF555/AF647 labeled Ure2-S53C measured by turbidity at OD_{400}. All the labeled proteins show similar aggregation kinetics to the unlabeled proteins. The conditions used were the same as in (**A**). The data shown are the average of three replicates, and the error bars represent the standard deviation of the mean. (**C**) TEM images of negatively stained fibrils of Ure2 and its variants. (i) WT Ure2. (ii) Ure2-V9C. (iii) Ure2-S53C. (iv) Ure2-S68C. (v) AF555/AF647 labeled Ure2-V9C. (vi) AF488/AF647 labeled Ure2-V9C. (vii) AF488/AF647 labeled Ure2-S53C. (viii) AF555/AF647 labeled Ure2-S68C. The scale bar is shown in each figure. All the images show similar fibril morphology. (**D**) SDS-PAGE analysis of Ure2 in the native state (N), and the supernatant (S) and pellet (P) fractions after fibril formation. Fibrils formed by unlabeled Ure2-V9C or Ure2-S68C (i) and AF555/AF647 labeled Ure2-V9C or Ure2-S68C (ii) were centrifuged at 14,000 *g* after the aggregation reaction reached a plateau. The pellet fraction was resuspended in an equal volume of buffer. Then 5 μL supernatant and resuspended pellet were mixed with 2×SDS loading buffer and either boiled at 95ºC for 5 min or used directly without boiling (labeled by *) before loading for SDS-PAGE. The results show that more than 90% of Ure2 is converted to amyloid fibrils.

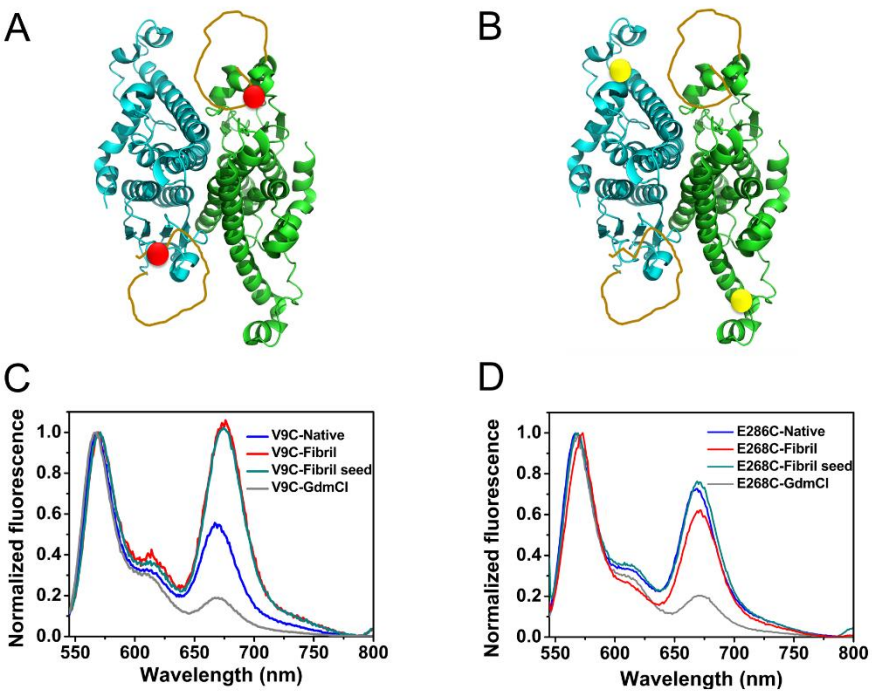

Figure S2. Ure2 dimers seldom dissociate into monomers during fibril formation as revealed by FRET between the two monomers within a dimer. Cy3/Cy5 double labeled Ure2 mixed with unlabeled Ure2 at a ratio of 1:20 was incubated to form fibrils, so that if dissociation during fibril formation occurs, the inter-dimer FRET signal will be lost (see SI Methods). (**A,B**) The labeling sites of V9C (**A**) and E268C (**B**) are indicated in the full-length Ure2 structure model. The labelling sites V9C and E268C are located in the N-terminal and C-terminal domain respectively. The FRET spectra for native Ure2, fibrillar Ure2, Ure2 fibril seeds and denatured Ure2 were measured. (**C**) The FRET spectra of Ure2-V9C before and after fibril formation. (**D**) The FRET spectra of Ure2-E268C before and after fibril formation. The unchanged FRET efficiency within the dimer of Ure2-E268C after fibrillization indicates that the Ure2 dimer does not dissociate into monomers when assembling into fibrils.

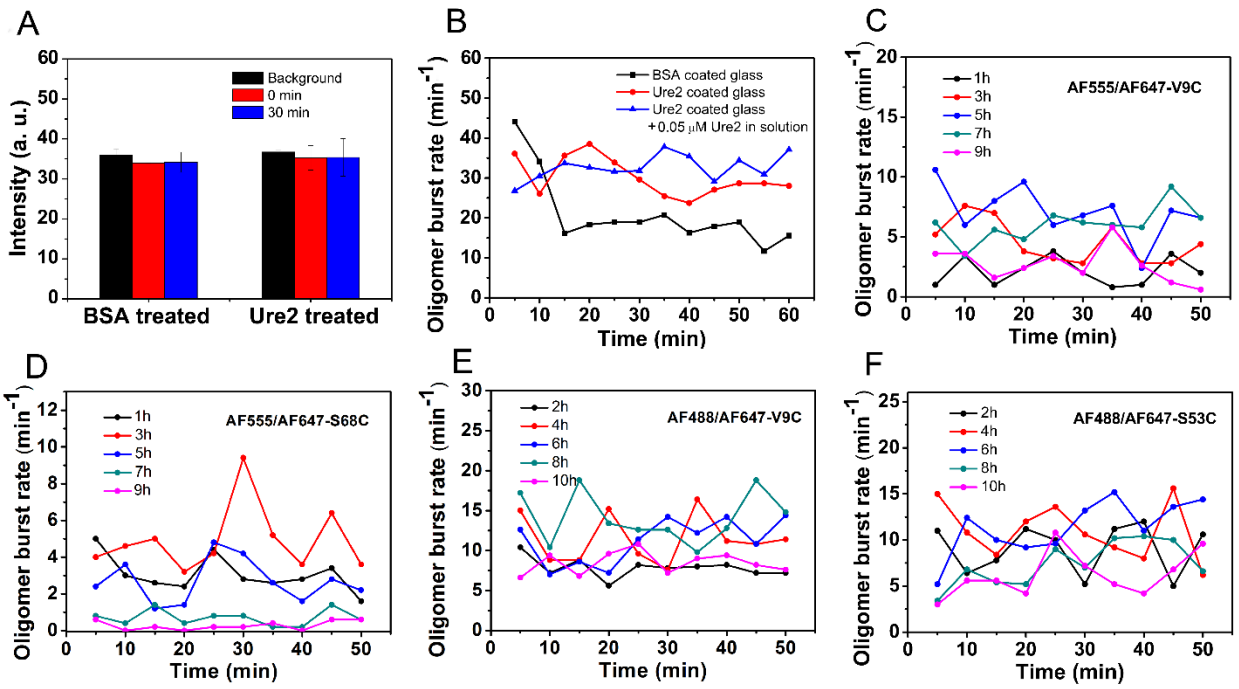

Figure S3. Estimation of the stability and dissociation of Ure2 oligomers upon dilution during the smFRET measurements. (**A**) Fluorescence intensity on BSA-coated and Ure2-coated surfaces measured by TIRF without (background, *black*) and upon the addition of a 15 μM equimolar mixture of AF488-labeled and AF647-labeled Ure2 initially (0 min, *red*) and after 30 min (*blue*). There is no significant difference between BSA and Ure2 treated surfaces compared with the background, indicating that both BSA and Ure2 can suppress protein adsorption on the coverslip. The results are the average of three independent measurements and the error bars represent the standard deviation of the mean. **(B)** Oligomer dissociation under different conditions monitored by confocal smFRET. AF555/AF647 labeled Ure2-V9C after 6 h incubation under fibril formation conditions was diluted 10^5-fold and measured by smFRET on coverslips treated in different ways. The coverslips were coated with 1 mg/ml BSA (black) or 5 μM unlabeled Ure2 (red) for 30 min before smFRET measurements. In addition, 0.05 μM unlabeled Ure2 was added to the diluted sample for measurement (blue), in order to check the dimer-dependent effect on oligomer dissociation. The rate of oligomer depletion in the absence of native Ure2 protection (ca. 66% within an hour) was consistent with the value for the dissociation rate constant obtained from fitting of smFRET data (see kinetic analysis section in the main text). **(C-F)** The oligomer burst rate of (**C**) AF555/AF647 labeled Ure2-V9C, (**D**) AF555/AF647 labeled Ure2-S68C, (**E**) AF488/AF647 labeled Ure2-V9C and (**F**) AF488/AF647 labeled Ure2-S53C averaged every 5 min was plotted against the measurement time, where the coverslips were pre-coated with 5 μM unlabeled Ure2. For each sample, five different time points during the aggregation reaction were chosen as representative. The results show that the oligomer concentration does not dramatically decrease upon dilution and remains at an almost constant level when using unlabeled Ure2 coated coverslips during the single molecule measurements.

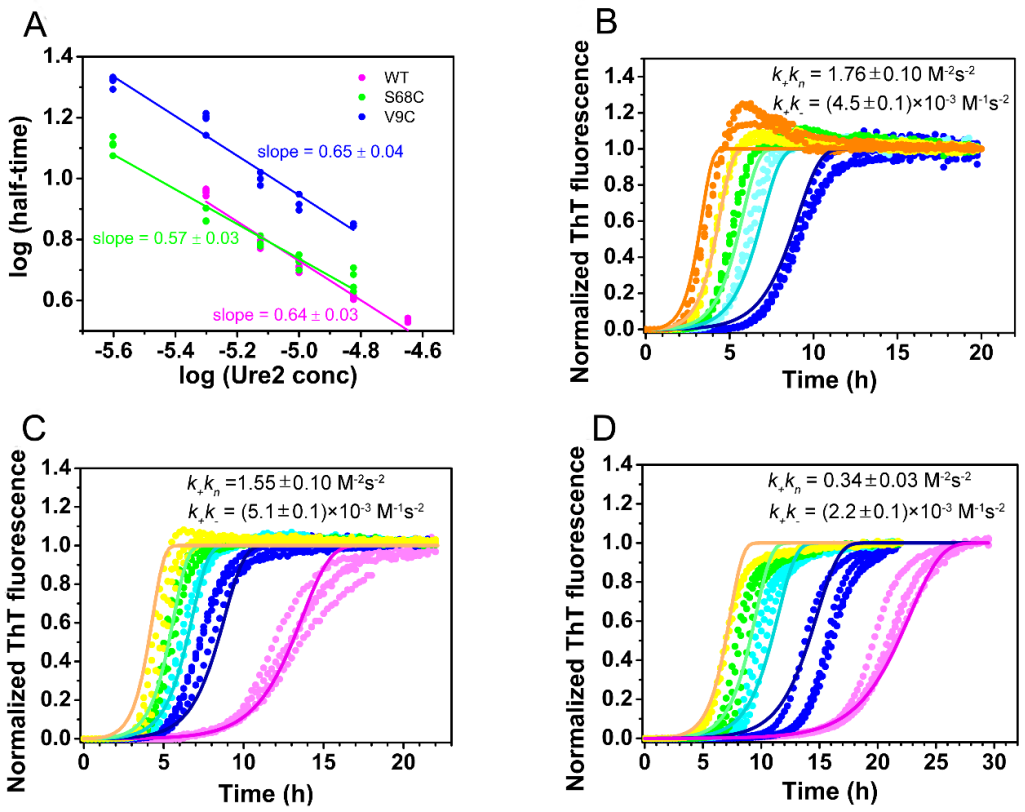

Figure S4. Global fitting of the kinetics of fibril formation of WT Ure2 and its variants. (**A**) Power-law scaling plot of half-time versus initial dimer concentration of WT (red), Ure2-S68C (green), Ure2-V9C (blue). The slopes give the scaling exponent of each protein. (**B-D**) The normalized ThT fluorescence curves of five concentrations of (**B**) WT Ure2, (**C**) Ure2-S68C and (**D**) Ure2-V9C were globally fitted using the analytical solution with a fragmentation-dominant mechanism (for details see SI Text). The concentrations shown in (**B-D**) are 2.5 μM (pink), 5 μM (blue), 7.5 μM (cyan), 10 μM (green), 15 μM (yellow), and 22.5 μM (orange). The ThT assay was carried out in a Fluostar Omega plate reader (BMGLabtech) at 30°C with 200 rpm orbital shaking. Three to five repetitions were analyzed for each concentration.

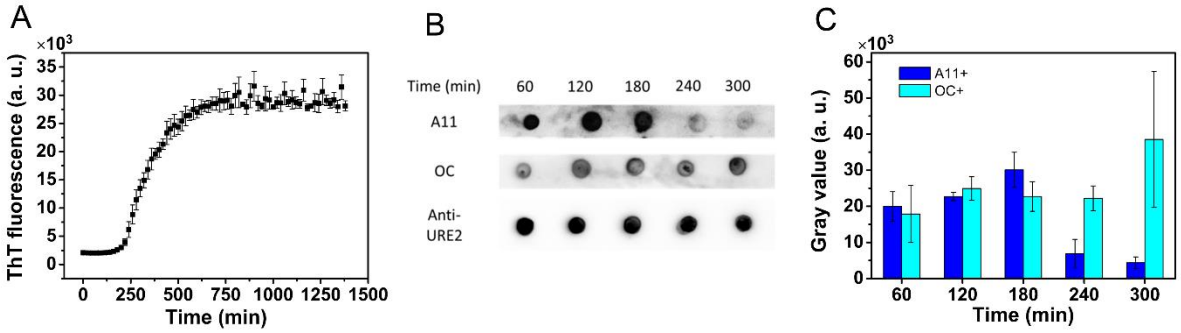

Figure S5. Dot blot analysis of the oligomers formed during fibril formation of the N-terminal prion domain (PrD) of Ure2 (residues 1-93). (**A**) Fibril formation of the PrD measured by ThT fluorescence. The ThT assay was carried out in a Fluostar Omega plate reader (BMGLabtech) at 30°C with 200 rpm orbital shaking. Error bars represent the standard deviation of the mean of three replicates. (**B**) A representative result of the dot blot analysis of oligomers formed during the early stages of PrD fibril formation. A 3 μL sample was removed from the solution and spotted on the membrane. The blots were probed with A11, OC and anti-Ure2 antibodies. (**C**) The time course of A11 and OC reactive oligomers during the early stages of PrD fibril formation measured by gray-scale of the blots. The results are the average of three independent replicates and the error bars represent the standard deviation of the mean.

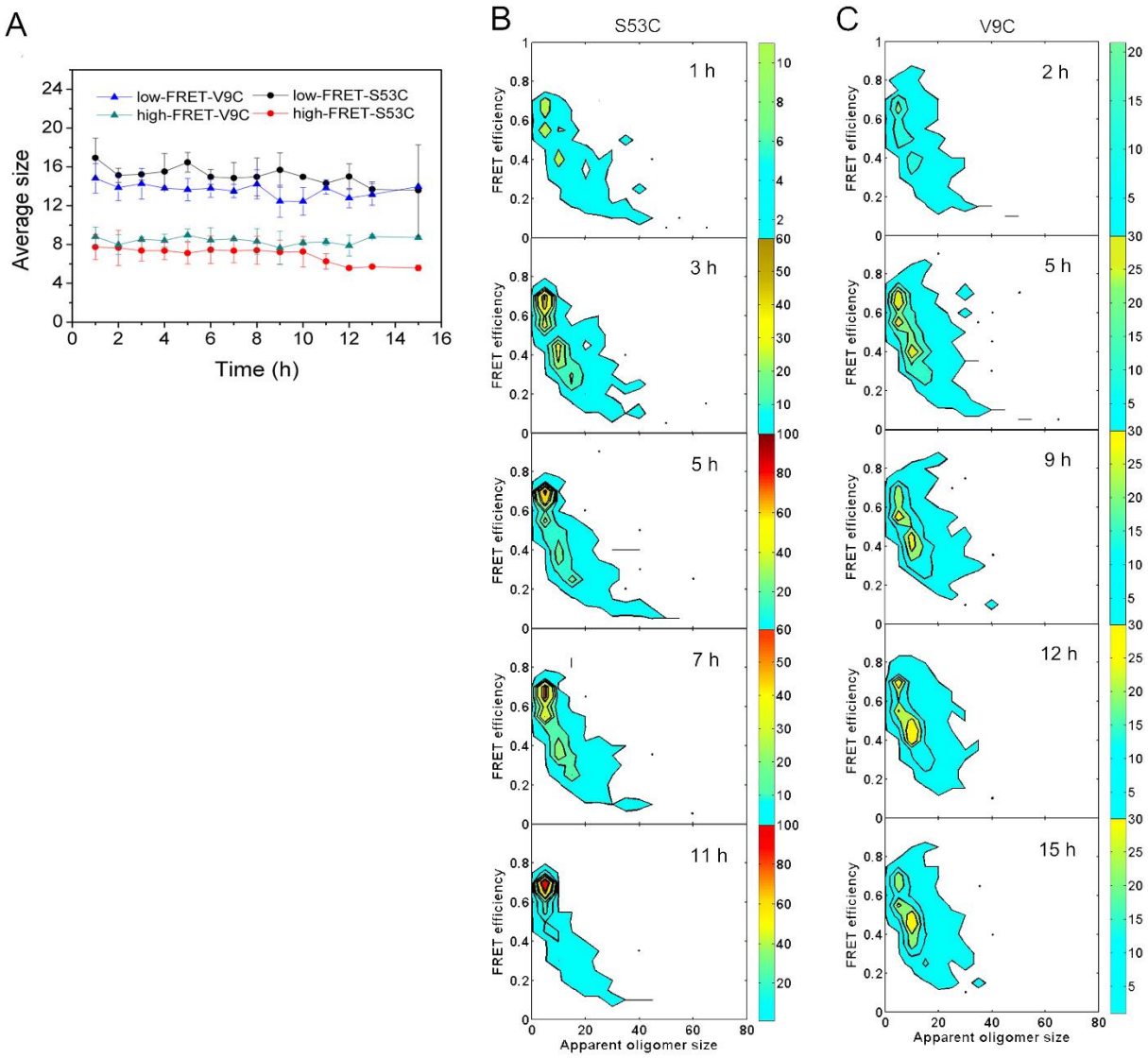

Figure S6. The apparent oligomer size analysis measured by single molecule FRET. (**A**) The average apparent size of low-FRET and high-FRET oligomers of Ure2-S53C and Ure2-V9C throughout the aggregation time. (**B-C**) Contour plots of FRET efficiency vs. apparent oligomer size distribution for (**B**) Ure2-S53C and (**C**) Ure2-V9C throughout the aggregation reaction measured by single molecule FRET**.** The apparent size was calculated by dividing the total burst intensity of the oligomers by the average intensity of AF488 labeled native Ure2 in the donor channel. The apparent oligomer size at different incubation times was plotted as a function of FRET efficiency to generate the 2D profile. The apparent average oligomer size and its distribution remained nearly constant throughout the aggregation reaction.

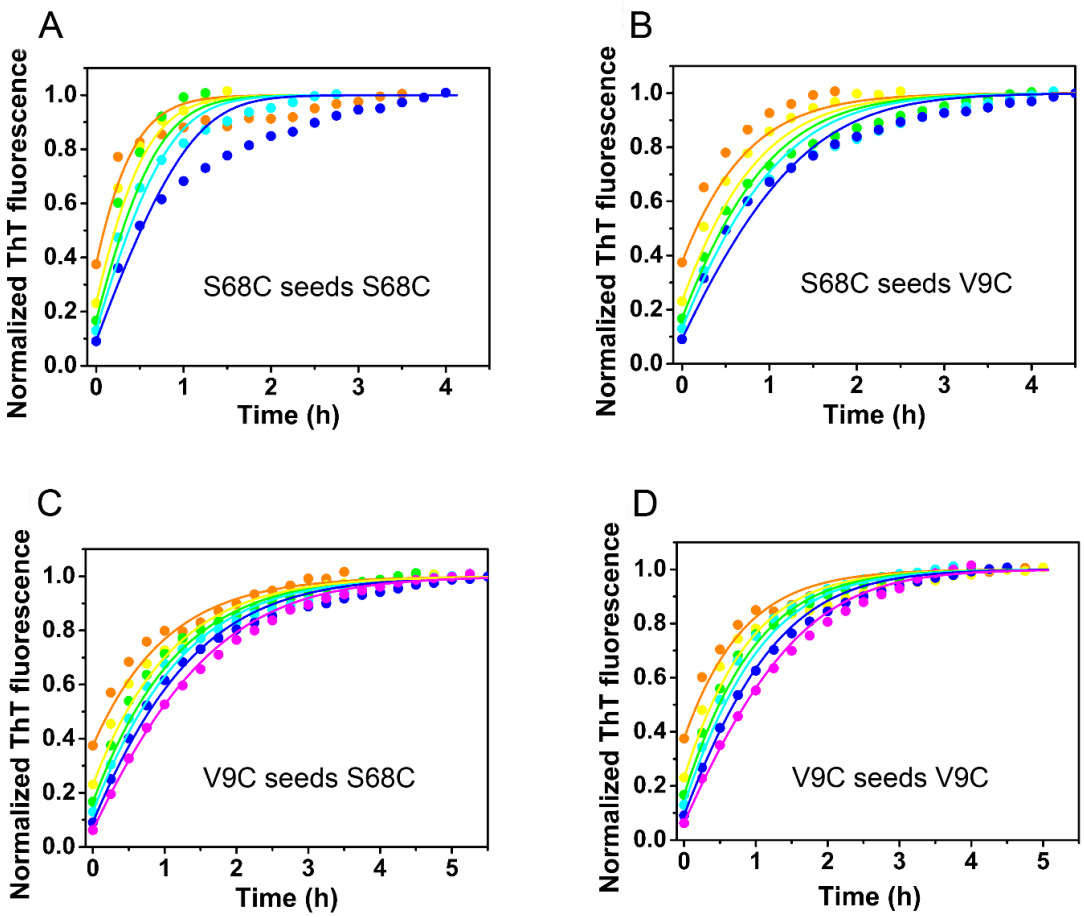

Figure S7. Fibril formation kinetics of self-seeding and cross-seeding of Ure2 variants monitored by ThT fluorescence. Solution of different concentrations of Ure2-S68C or Ure2-V9C, 2.5 μM (orange), 5 μM (yellow), 7.5 μM (green), 10 μM (cyan), 15 μM (blue), 22.5 μM (pink), were incubated with 1.5 μM fibril seeds of Ure2-S68C or Ure2-V9C as indicated in the figure. The seeding experiments were carried out in a Fluostar Omega plate reader (BMGLabtech) at 18°C with 200 rpm orbital shaking. The data were globally fitted to the saturation-elongation model to obtain the ratio of the initial elongation rate constants for the two protein variants and an estimation of the individual elongation rate constants.

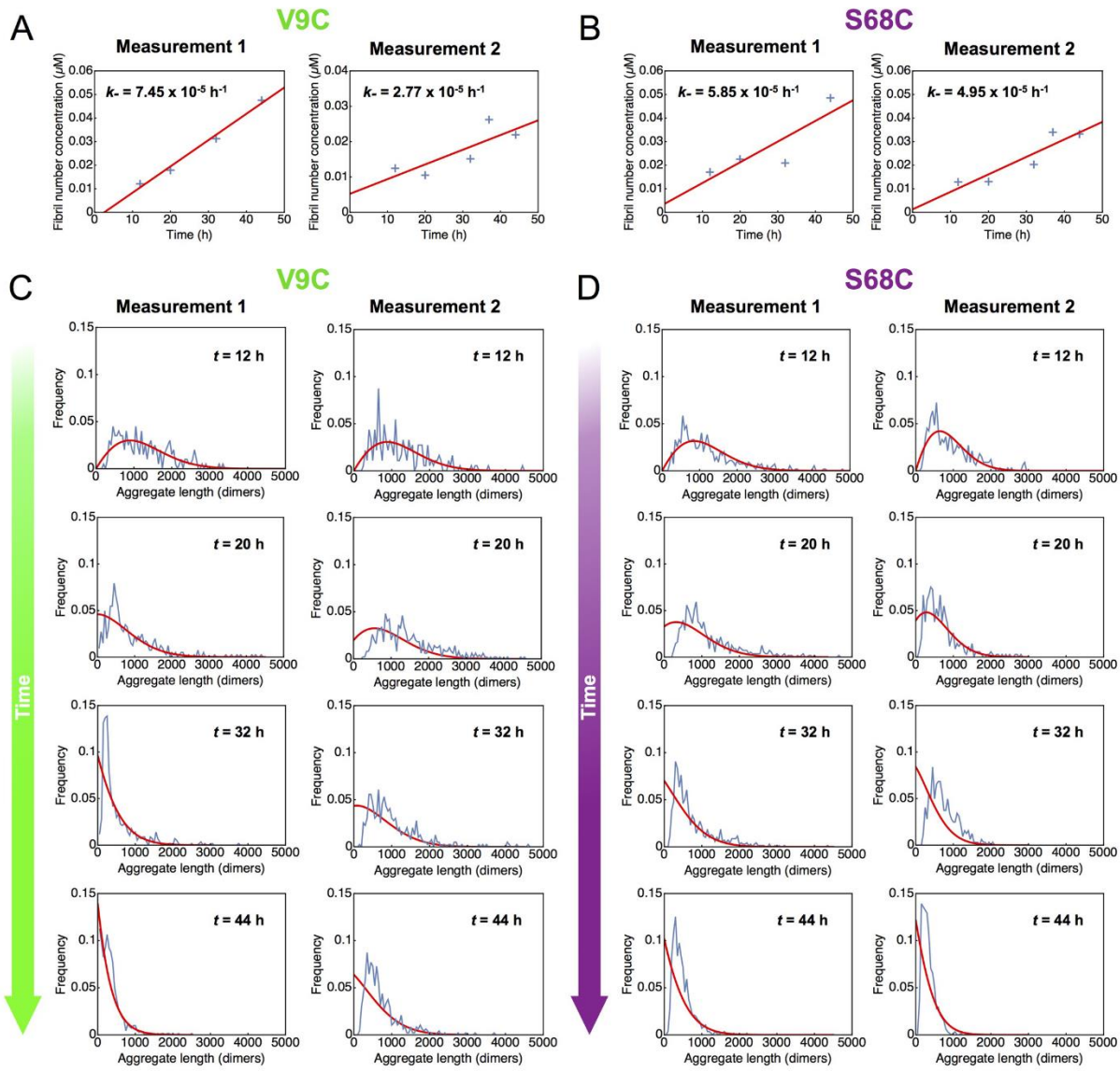

Figure S8. Kinetic analysis of fibril length distributions to determine fragmentation rates. (**A,B**) Time evolution of fibril concentration *P* for each protein variant, as determined from the average length, is fitted to a straight line, whose slope yields the fragmentation rate constant (see ***Determining fragmentation rates from analysis of fibril length distributions*** above). (**C,D**) The extracted fragmentation rate constants were used to generate predictions for the time evolution of the full aggregate length distribution, matching the experimental data well.

Table S1. Fitting results of kinetic analysis of Ure2 variants using different threshold criteria.

	Threshold (D=10 and A=20)			Threshold (D=10 and A=10)		
	S68C	V9C	Ratio	S68C	V9C	Ratio
k_{oligo} /$\mu M^{-1}h^{-1}$	1.6×10^{-4}	1.6×10^{-4}	1	2.6×10^{-4}	2.6×10^{-4}	1
k_d /h^{-1}	0.60	0.45	1.3	0.65	0.42	1.5
k_c /h^{-1}	2.3×10^{-3}	1.6×10^{-3}	1.4	2.0×10^{-3}	1.4×10^{-3}	1.4
k_+ /$\mu M^{-1}h^{-1}$	50	33	1.5	50	33	1.5
k_- /h^{-1}	1.2×10^{-4}	1.2×10^{-4}	1	7.1×10^{-5}	7.1×10^{-5}	1

Table S2. Sensitivity analysis for varying oligomer formation reaction orders.

	Fitted Parameter Values			Precision
	n_o = 2 (default)	n_o = 1	n_o = 3	
k_- /h^{-1}	1.2×10^{-4}	1.4×10^{-4}	1.2×10^{-4}	OM[a]
$k_{oligo}m(0)^{n_o}$ /$\mu M\ h^{-1}$	3.6×10^{-2}	4.6×10^{-2}	2.9×10^{-2}	$\pm0.3\times10^{-2}$
k_c (S68C) /h^{-1}	2.3×10^{-3}	2.0×10^{-3}	2.3×10^{-3}	OM[a]
k_c (V9C) /h^{-1}	1.7×10^{-3}	1.5×10^{-3}	1.6×10^{-3}	OM[a]
k_c ratio	1.4	1.3	1.4	±0.3
k_d (S68C) /h^{-1}	0.60	0.89	0.47	±0.08
k_d (V9C) /h^{-1}	0.45	0.67	0.36	±0.05
k_d ratio	1.3	1.3	1.3	±0.3
Fitting error /MRE[b]	1.6	2.1	1.4	

[a] OM, order-of-magnitude precision.

[b] MRE, mean residual error.

Table S3. Sensitivity analysis for varying V9C oligomer conversion reaction orders n_p (V9C), with S68C conversion reaction order n_p (S68C) = 0.

	Fitted Parameter Values			Error
	n_p (V9C) = 0	n_p (V9C) = 1	n_p (V9C) = 3	
k_- /h^{-1}	1.2×10^{-4}	1.2×10^{-4}	1.3×10^{-4}	OM[a]
k_{oligo} /$\mu M^{-1}\ h^{-1}$	1.6×10^{-4}	1.6×10^{-4}	1.6×10^{-4}	$\pm0.1\times10^{-4}$
$k_cm(0)^{n_p}$ (S68C) /$\mu M\ h^{-1}$	2.3×10^{-3}	2.2×10^{-3}	2.1×10^{-3}	OM[a]
$k_cm(0)^{n_p}$ (V9C) /$\mu M\ h^{-1}$	1.7×10^{-3}	1.7×10^{-3}	1.7×10^{-3}	OM[a]
$k_cm(0)^{n_p}$ ratio	1.4	1.3	1.2	±0.3
k_d (S68C) /h^{-1}	0.60	0.60	0.61	±0.08
k_d (V9C) /h^{-1}	0.45	0.45	0.45	±0.05
k_d ratio	1.3	1.3	1.3	±0.3
Fitting error /MRE[b]	1.6	1.6	1.6	

[a] OM, order-of-magnitude precision.

[b] MRE, mean residual error.

Table S4. Sensitivity analysis for varying V9C oligomer conversion reaction orders n_p (V9C), with S68C conversion reaction order n_p (S68C) = 1.

	Fitted Parameter Values			Error
	n_p (V9C) = 0	n_p (V9C) = 1	n_p (V9C) = 3	
k_-/h^{-1}	1.2×10^{-4}	1.2×10^{-4}	1.3×10^{-4}	OM[a]
k_{oligo} /μM^{-1} h^{-1}	1.6×10^{-4}	1.6×10^{-4}	1.6×10^{-4}	$\pm0.1\times10^{-4}$
$k_c m(0)^{n_p}$ (S68C) /μM h^{-1}	2.4×10^{-3}	2.3×10^{-3}	2.2×10^{-3}	OM[a]
$k_c m(0)^{n_p}$ (V9C) /μM h^{-1}	1.7×10^{-3}	1.7×10^{-3}	1.7×10^{-3}	OM[a]
$k_c m(0)^{n_p}$ ratio	1.5	1.4	1.3	±0.3
k_d (S68C) /h^{-1}	0.59	0.60	0.60	±0.08
k_d (V9C) /h^{-1}	0.45	0.45	0.45	±0.05
k_d ratio	1.3	1.3	1.3	±0.3
Fitting error /MRE[b]	1.6	1.6	1.6	

[a] OM, order-of-magnitude precision.

[b] MRE, mean residual error.

Table S5. Sensitivity analysis for varying V9C oligomer conversion reaction orders n_p (V9C), with S68C conversion reaction order n_p (S68C) = 3.

	Fitted Parameter Values			Error
	n_p (V9C) = 0	n_p (V9C) = 1	n_p (V9C) = 3	
k_- /h^{-1}	1.2×10^{-4}	1.2×10^{-4}	1.3×10^{-4}	OM[a]
k_{oligo} /μM^{-1} h^{-1}	1.6×10^{-4}	1.6×10^{-4}	1.6×10^{-4}	$\pm0.1\times10^{-4}$
$k_c m(0)^{n_p}$ (S68C) /μM h^{-1}	2.7×10^{-3}	2.5×10^{-3}	2.4×10^{-3}	OM[a]
$k_c m(0)^{n_p}$ (V9C) /μM h^{-1}	1.7×10^{-3}	1.7×10^{-3}	1.7×10^{-3}	OM[a]
$k_c m(0)^{n_p}$ ratio	1.6	1.5	1.4	±0.3
k_d (S68C) /h^{-1}	0.59	0.59	0.60	±0.08
k_d (V9C) /h^{-1}	0.45	0.45	0.45	±0.05
k_d ratio	1.3	1.3	1.3	±0.3
Fitting error /MRE[b]	1.6	1.6	1.6	

[a] OM, order-of-magnitude precision.

[b] MRE, mean residual error.

References

(1) Fei, L.; Perrett, S. *J Biol Chem* **2009**, *284*, 11134-11141.

(2) Lou, F.; Yang, J.; Wu, S.; Perrett, S. *Chem Comm* **2017**, *53*, 7986-7989.

(3) Cremades, N.; Cohen, S. I.; Deas, E.; Abramov, A. Y.; Chen, A. Y.; Orte, A.; Sandal, M.; Clarke, R. W.; Dunne, P.; Aprile, F. A.; Bertoncini, C. W.; Wood, N. W.; Knowles, T. P.; Dobson, C. M.; Klenerman, D. *Cell* **2012**, *149*, 1048-1059.

(4) Narayan, P.; Orte, A.; Clarke, R. W.; Bolognesi, B.; Hook, S.; Ganzinger, K. A.; Meehan, S.; Wilson, M. R.; Dobson, C. M.; Klenerman, D. *Nat Struct Mol Biol* **2012**, *19*, 79-83.

(5) Hoffmann, A.; Kane, A.; Nettels, D.; Hertzog, D. E.; Baumgartel, P.; Lengefeld, J.; Reichardt, G.; Horsley, D. A.; Seckler, R.; Bakajin, O.; Schuler, B. *Proc Natl Acad Sci U S A* **2007**, *104*, 105-110.

(6) Roy, R.; Hohng, S.; Ha, T. *Nat Methods* **2008**, *5*, 507-516.

(7) Preus, S.; Noer, S. L.; Hildebrandt, L. L.; Gudnason, D.; Birkedal, V. *Nat Methods* **2015**, *12*, 593-594.

(8) Michaels, T. C. T.; Knowles, T. P. J. *Int J Mod Phys B* **2015**, *29*, 153002.

(9) Garcia, G. A.; Cohen, S. I.; Dobson, C. M.; Knowles, T. P. *Phys Rev E Stat Nonlin Soft Matter Phys* **2014**, *89*, 032712.

(10) Knowles, T. P.; Waudby, C. A.; Devlin, G. L.; Cohen, S. I.; Aguzzi, A.; Vendruscolo, M.; Terentjev, E. M.; Welland, M. E.; Dobson, C. M. *Science* **2009**, *326*, 1533-1537.

(11) Burnham, K. P.; Anderson, D. R. *Model selection and multimodel inference : a practical information-theoretic approach*; Springer New York, 2003.

(12) Meisl, G.; Kirkegaard, J. B.; Arosio, P.; Michaels, T. C.; Vendruscolo, M.; Dobson, C. M.; Linse, S.; Knowles, T. P. *Nat Protoc* **2016**, *11*, 252-272.

(13) Zhang, Z. R.; Perrett, S. *J Biol Chem* **2009**, *284*, 14058-14067.

(14) Galani, D.; Fersht, A. R.; Perrett, S. *J Mol Biol* **2002**, *315*, 213-227.

(15) Cohen, S. I.; Vendruscolo, M.; Dobson, C. M.; Knowles, T. P. *J Mol Biol* **2012**, *421*, 160-171.

(16) Cohen, S. I.; Vendruscolo, M.; Welland, M. E.; Dobson, C. M.; Terentjev, E. M.; Knowles, T. P. *J Chem Phys* **2011**, *135*, 065105.

(17) Glabe, C. G. *J Biol Chem* **2008**, *283*, 29639-29643.

(18) Kayed, R.; Head, E.; Sarsoza, F.; Saing, T.; Cotman, C. W.; Necula, M.; Margol, L.; Wu, J.; Breydo, L.; Thompson, J. L.; Rasool, S.; Gurlo, T.; Butler, P.; Glabe, C. G. *Mol Neurodegener* **2007**, *2*, 18.

(19) Krishnan, R.; Goodman, J. L.; Mukhopadhyay, S.; Pacheco, C. D.; Lemke, E. A.; Deniz, A. A.; Lindquist, S. *Proc Natl Acad Sci U S A* **2012**, *109*, 11172-11177.

(20) Xue, W. F.; Radford, S. E. *Biophys J* **2013**, *105*, 2811-2819.

(21) Michaels, T. C.; Yde, P.; Willis, J. C.; Jensen, M. H.; Otzen, D.; Dobson, C. M.; Buell, A. K.; Knowles, T. P. *J Chem Phys* **2015**, *143*, 164901.